Deposition and characterization of highly oriented $Mg_3(VO_4)_2$ thin film catalysts. 2. Controlled variation of oxygen content

Allen G. Sault [a], Judith A. Ruffner [b] and Jason E. Mudd [a]

[a] *Catalytic and Porous Materials Department, Sandia National Laboratories, Albuquerque, NM 87185-1349, USA*
[b] *Electronic and Optical Materials Department, Sandia National Laboratories, Albuquerque, NM 87185-1349, USA*

Received 26 April 2001; accepted 20 July 2001

Thin films of magnesium vanadates oriented to expose a single crystalline face, could potentially serve as ideal models for high surface area magnesium vanadate catalysts for oxidative dehydrogenation. The growth of oriented films of one particular magnesium vanadate phase, the orthovanadate ($Mg_3(VO_4)_2$), has been achieved by rf sputter deposition of the orthovanadate onto Au(111) surfaces. X-ray diffraction, Fourier transform infrared spectroscopy, and X-ray photoelectron spectroscopy have been used to investigate the structure and composition of the films. The orthorhombic orthovanadate grows epitaxially with the (021) plane oriented parallel to the surface. By varying oxygen flow rates during deposition the stoichiometry of the films can be varied from fully oxidized to highly oxygen deficient. At very low oxygen flow rates or in the complete absence of oxygen, a reduced $Mg_3V_2O_6$ phase is formed. This reduced phase has a cubic structure and grows with the (100) plane parallel to the surface.

KEY WORDS: magnesium vanadate; oxidative hydrogenation; thin film catalyst; model catalyst

1. Introduction

Small alkenes such as ethene and propene are currently synthesized *via* steam cracking of small alkanes [1]. The large energy costs and low selectivities associated with this process motivates a search for more energy efficient processes. Potential alternatives include both oxidative and nonoxidative catalytic dehydrogenation. In nonoxidative dehydrogenation, thermal treatment of the alkane over a catalyst produces the alkene and hydrogen according to the reaction

$$C_nH_{2n+2} \rightarrow C_nH_{2n} + H_2 \quad (1)$$

This endothermic reaction is equilibrium limited, necessitating high temperatures and low pressures to achieve adequate conversions. High temperatures not only require large energy input, but also decrease selectivity by promoting cracking reactions and coke formation. In contrast, oxidative dehydrogenation (ODH) reacts the alkane with oxygen according to the reaction

$$C_nH_{2n+2} + O_2 \rightarrow C_nH_{2n} + H_2O \quad (2)$$

Unlike nonoxidative dehydrogenation, ODH is exothermic and, therefore, not equilibrium limited, offering the possibility of low temperature operation, minimal carbon deposition, and substantial energy savings. Of course, the thermodynamics of alkane/oxygen systems favors complete combustion to CO_2 and water, so achievement of high selectivity is a major challenge for ODH.

Mixed metal oxides are the most promising candidates for practical ODH catalysts. In all active mixed metal oxide systems, multiple crystalline phases are known and synergistic effects between phases are often reported. One commonly studied system, particularly for propane ODH, is comprised of the magnesium vanadates. Three fully oxidized magnesium vanadate phases exist: $Mg_3(VO_4)_2$ (orthovanadate), $Mg_2V_2O_7$ (pyrovanadate), and MgV_2O_6 (metavanadate). In addition, a reduced $Mg_3V_2O_6$ phase has been reported [2], which was earlier observed but only identified as a cubic orthovanadate phase [3]. The preponderance of evidence suggests that the pyrovanadate is a superior propane ODH catalyst in comparison to the other two phases, but a recognized strong effect of catalyst preparation methods on performance makes it difficult to draw definitive conclusions regarding relative performance [4–6]. Furthermore, synergistic interactions between phases give rise to multiphase catalysts with performance superior to that of any of the individual phases [7]. Coupling the uncertainty regarding relative activity of the different phases with an almost complete lack of knowledge regarding which crystalline planes of the various phases are exposed in active catalysts renders identification of active sites extremely difficult.

Studies with well defined model catalysts would help to clarify this situation. In this paper we report on continuing efforts to develop such model systems. Ideally, one would use single crystals of the mixed metal oxides, cut and polished to expose a single crystal plane, as model systems. This possibility is limited, however, both by the difficulty of growing high quality single crystals of mixed metal oxides, as well as the insulating nature of the oxides which complicates the analysis of data from typical ultrahigh vacuum (UHV) surface analytical probes. In the case of simple

oxides, such as alumina, magnesia, and iron oxides, various workers [8–10] have utilized thin oxide films grown epitaxially on suitable substrates to overcome these problems. The films are thick enough to mimic the behavior of bulk materials, but thin enough so that they do not support static charging during surface analysis, to the point that scanning tunneling microscopy (STM) can be performed on the surfaces. We are developing analogous methods to epitaxially deposit oriented thin films of magnesium vanadates consisting of a single crystalline phase and exposing only a single crystal plane.

Our initial efforts in this area involved the formation of thin films of magnesium orthovanadate exposing only the (021) plane [11]. Although the magnesium orthovanadate structure is orthorhombic, consideration of the oxygen ions alone reveals a pseudo-cubic arrangement [12], with the magnesium and vanadium ions occupying select octahedral and tetrahedral sites, respectively. The (021) plane of $Mg_3(VO_4)_2$ is parallel to the close-packed layers of oxygen ions, and therefore displays a distorted hexagonal symmetry, as shown in figure 1.

The symmetry of the $Mg_3(VO_4)_2$ (021) surface is well matched by the (111) surfaces of fcc metals, and epitaxial growth of $Mg_3(VO_4)_2$ (021) surface could be expected on an fcc (111) metal surface with atomic spacing equal to the average O–O bond distance in the $Mg_3(VO_4)_2$ (021) surface. Among the several metals that meet this requirement, Au(111) provides an excellent substrate. In addition to a good epitaxial match, gold is also highly inert and does not react with the overlying $Mg_3(VO_4)_2$ (021) layer [11]. In previous work [11], we reported our initial efforts to sputter deposit epitaxial $Mg_3(VO_4)_2$ (021) films onto Au(111) surfaces, and demonstrated that both the desired Mg : V ratio and crystalline orientation were achieved. In this work we investigate the effects of oxygen flow rate during deposition on film quality. Specifically, we show that films ranging from fully oxidized $Mg_3(VO_4)_2$ to heavily reduced $Mg_3V_2O_6$ can be produced depending upon deposition conditions. Elsewhere we will report on the chemical response of our films under conditions encountered during ODH reactions [13].

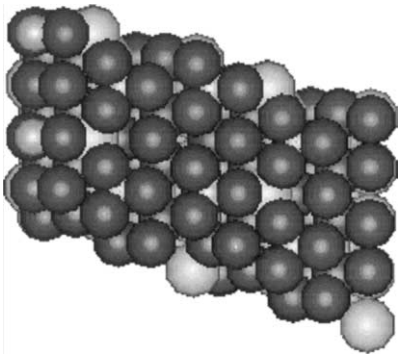

Figure 1. Oxygen terminated (021) surface of $Mg_3(VO_4)_2$, showing hexagonal symmetry. The dark gray spheres in the top layer are oxygen atoms, and the light gray spheres in the second layer are V and Mg ions in octahedral and tetrahedral sites, respectively.

2. Experimental

Full details of the film deposition process are provided elsewhere [11], so only a brief overview of the procedures is given here. Au(111) substrates were obtained by DC sputter deposition of 50 nm gold films onto polished Si wafers at room temperature. The wafers were covered by a 4000 Å thick thermally grown oxide layer. By employing oxidized Si wafers, we avoid reaction between Si and Au to form silicides. Au films naturally align themselves to expose the desired (111) surface since the close-packed arrangement of oxygen atoms in this plane maximizes coordination number at the surface and minimizes surface free energy. This alignment of the Au film occurs despite the amorphous nature of the underlying oxidized Si layer. Note that the Au(111) substrate formed by this procedure is not a single crystal surface, but rather a polycrystalline surface in which the exposed (111) surfaces of each crystallite are rotationally disordered with respect to each other. Preliminary atomic force microscopy (AFM) images suggest that the crystallites are on the order of 30–40 nm in size.

200 nm thick $Mg_3(VO_4)_2$ films were deposited onto the Au substrates at 573 K using reactive rf sputtering from a stoichiometric ceramic target. A nominal deposition rate of 6.4 nm/min was employed and oxygen flow rate during deposition was varied from 0.0 to 7.5 sccm. Our previous work provides further details of the deposition process, extensive X-ray diffraction (XRD) analysis demonstrating that the desired (021) film orientation is achieved by our deposition process, and chemical analysis showing achievement of the proper Mg : V stoichiometry. Like the Au(111) substrates the oriented $Mg_3(VO_4)_2$ films are not single crystals, but rather polycrystalline surfaces with random rotational orientation of the individual exposed (021) planes.

Film structure and composition were analyzed by XRD, Fourier transform infrared (FTIR) spectroscopy, and X-ray photoelectron spectroscopy (XPS). XRD was performed using standard θ–2θ X-ray diffraction on a Siemens D-500 XRD. A Nicolet 20SXB Fourier transform infrared spectrometer equipped with a SpectraTech COLLECTOR^{TM} diffuse reflectance accessory was used to obtain FTIR spectra of the films. Although this accessory is not designed for specular reflectance measurements, we have found that high quality reflectance spectra can be obtained provided that the angle of incidence is adjusted so that the IR beam penetrates the film and is reflected off the underlying gold layer rather than off the surface of the $Mg_3(VO_4)_2$ films. Samples were mounted by placing a small piece of the coated Si wafer on top of the diffuse reflectance sample cup and adjusting the optics to maximize signal. Background spectra were obtained from an oxidized Si wafer coated with a 50 nm Au film, deposited in an identical fashion to those used as substrates for the $Mg_3(VO_4)_2$ films.

XPS was performed using a VG Microtech Clam 2 operated at an analyzer resolution of 1.0 eV, with excitation provided by a VG Microtech XR3 Al Kα X-ray source. Iden-

tification of V oxidation states by XPS is somewhat problematic, as pointed out by Gao *et al.* [6]. While the $2p_{3/2}$ binding energy of V^{5+} is generally agreed to be between 517.1 and 517.6 eV, discrimination between V^{4+} and V^{3+} is not as clear. Gao *et al.* [6] assign a peak at 515.5 eV to V^{4+}, but in the present work we assign this peak to V^{3+} since it appears in samples that are known by XRD to contain V^{3+} in the form of $Mg_3V_2O_6$ (see below). Also, Burrows *et al.* [14] report V^{3+} formation, but no V^{4+}, upon reduction of $Mg_3(VO_4)_2$ in a rich propane/oxygen environment. Nevertheless, the possibility of some V^{4+} at the surface of reduced samples cannot be completely discounted. For fully oxidized films, binding energies were referenced to the V $2p_{3/2}$ peak at 517.6 eV, corresponding to V^{5+}. Fully oxidized films were identified by the presence of a sharp, symmetrical V $2p_{3/2}$ peak 13.0 ± 0.1 eV below the O 1s peak. Oxygen deficient films generally display a broad peak consisting of both V^{5+} and V^{3+}. The oxygen deficient films also have a relatively high electrical conductivity, and do not exhibit any charging during XPS.

For comparison purposes, a powder sample of $Mg_3(VO_4)_2$ was prepared using the citrate method described by Delmon and coworkers [6,15]. A transparent solution of $Mg(NO_3)_2$ and NH_4VO_3 in the proper stoichiometric ratio was treated with citric acid in an amount to give a 10% molar excess of anions over cations. The solution was evaporated in a rotovap at 40 °C to obtain a viscous material and then dried at 80–90 °C to obtain a solid. The dry solid was decomposed in air at 380 °C for 18 h and then calcined at 550 °C for 6 h. The resulting powder possesses a surface area of 25.5 m^2/g and gives the powder XRD pattern expected for $Mg_3(VO_4)_2$ with no detectable impurities. An FTIR spectrum of the $Mg_3(VO_4)_2$ powder was obtained by mixing the powder with ground KBr to give 5 wt% orthovanadate, and then filling the sample cup of the FTIR diffuse reflectance accessory with the mixture. $Mg_3(VO_4)_2$ powder absorbs IR light so strongly that unacceptably low transmission is obtained unless the powder is diluted. KBr is a commonly used diluent since it is a good diffuse reflector that does not absorb infrared radiation. A background for the $Mg_3(VO_4)_2$ powder spectrum was obtained from pure KBr powder.

3. Results and discussion

Figure 2 shows XRD of the oriented films as a function of oxygen flow rate during deposition. For films deposited with oxygen flow rates of 1.0 sccm or greater, XRD shows a peak at $2\theta = 38.17°$, corresponding to a lattice spacing (d) of ~2.35 Å. This peak is a combination of the Au(111) and $Mg_3(VO_4)_2$ (042) diffraction peaks, as demonstrated in earlier work [11]. Peaks corresponding to Si(400) from the substrate are the only other features observed. For oxygen flow rates below 1.0 sccm an additional peak appears at $2\theta = 42.95°$ ($d \approx 2.10$ Å). This peak corresponds to the (400) diffraction peak of the reduced $Mg_3V_2O_6$ phase [2], indicating that these films are highly oxygen deficient, and that the (100) planes of $Mg_3V_2O_6$ are exposed.

XPS experiments support the formation of $Mg_3V_2O_6$ at low oxygen flow rates (see figure 3). While the film prepared in the absence of oxygen initially displays a mixture of V^{5+} (517.6 eV) and V^{3+} (515.6 eV) near the surface (figure 3(A)), mild heating in vacuum to 673 K for 5 min results in complete conversion of all near-surface vanadium to V^{3+} (figure 3(B)). Films deposited with oxygen flow rates above 1.0 sccm show only V^{5+} initially (figure 3(C)), and little or no conversion to reduced V upon heating in vacuum (figure 3(D)). These results are entirely consistent with formation of $Mg_3V_2O_6$ in the film deposited in the absence of oxygen. Exposure of the film to air upon removal from the deposition chamber oxidizes any reduced V formed in the near-surface region during deposition, resulting in observation of V^{5+} by XPS even though the as-deposited film contains only V^{3+}. Mild heating in vacuum easily reverses the surface oxidation through oxygen desorption and/or diffusion into the bulk, converting V^{5+} in the near-surface region back to V^{3+}. For fully oxidized films, mild heating in vacuum also likely results in oxygen desorption, but in this

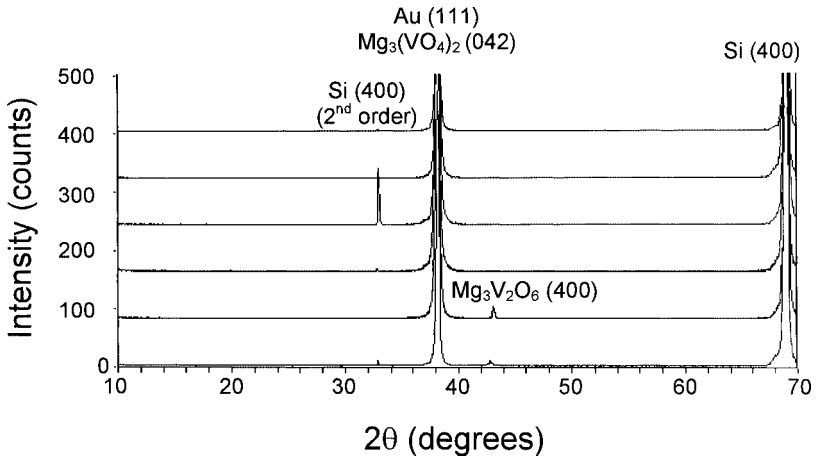

Figure 2. XRD of magnesium vanadate films as a function of oxygen flow rate. Oxygen flow rates from bottom to top are (a) 0.0, (b) 0.3, (c) 1.0, (d) 2.5, (e) 5.0 and (f) 7.5 sccm.

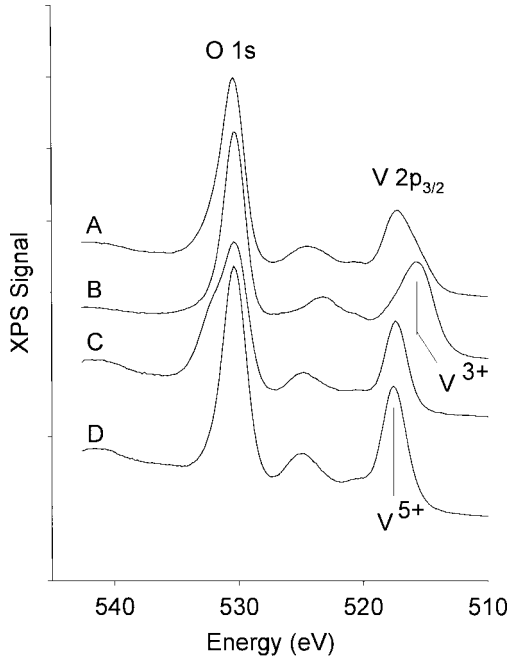

Figure 3. V 2p and O 1s XPS of magnesium vanadate films: (A) film prepared with 0.0 sccm O_2, (B) film prepared with 0.0 sccm O_2 after heating to 673 K in vacuum for 5 min (C) film prepared with 5.0 sccm O_2, (D) film prepared with 5.0 sccm O_2 after heating to 673 K in vacuum for 5 min.

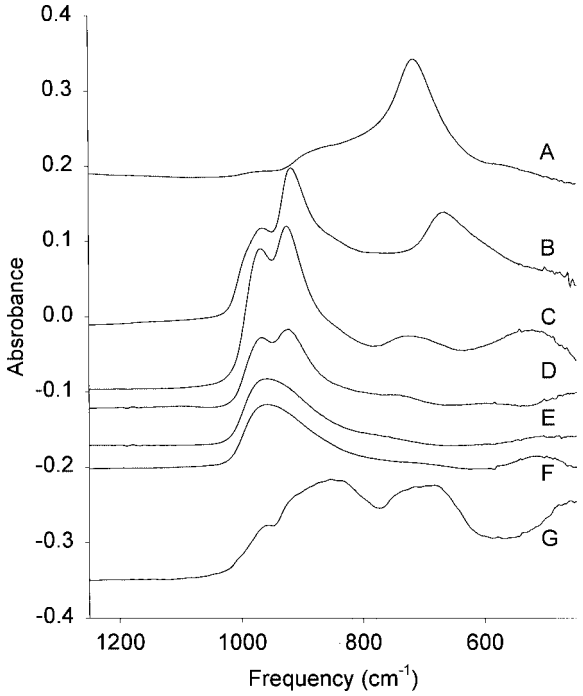

Figure 4. FTIR spectra of (021) oriented magnesium vanadate films as a function of oxygen flow rate: (A) 0.0, (B) 0.3, (C) 1.0, (D) 2.5, (E) 5.0 and (F) 7.5 sccm; (G) magnesium orthovanadate powder.

case the oxygen vacancies diffuse into the bulk and the corresponding reduced V species are found throughout the bulk of the film rather than at the surface.

The formation of oxygen vacancies during deposition is also reflected in the electrical conductivity of the films. Pantazidis *et al.* [16] have shown that reduction of $Mg_3(VO_4)_2$ results in order of magnitude increases in bulk electrical conductivity, and that the conductivity can be ascribed to anionic oxygen vacancies. We see similar changes in the conductivity of our films as the extent of oxidation decreases. Fully oxidized films exhibit moderate sample charging during XPS, resulting in binding energy shifts of $\sim$2 eV indicative of relatively low conductivity. Highly oxygen deficient films exhibit no charging, indicating a substantial increase in conductivity. For the sample deposited with 2.5 sccm O_2 an intermediate behavior occurs; the film initially exhibits modest charging of 0.9 eV, but after heating in vacuum charging no longer occurs. Thus, oxygen vacancy concentration clearly increases as oxygen flow rate decreases.

FTIR measurements shed further light on the extent of oxidation of the films. Figure 4 shows FTIR reflectance spectra of the films along with a diffuse reflectance spectrum of the orthovanadate powder for comparison. These spectra show major changes in vibrational properties as oxygen content increases. In contrast to XRD, which shows no changes for oxygen flow rates above 1.0 sccm, FTIR shows continued changes until a flow rate of 5.0 sccm is reached, indicating that fully oxidized films are not formed below this flow rate. A future publication dealing with response of the films to exposure to reactive conditions [13] will show significant differences between films deposited with 5.0 and 7.5 sccm O_2, suggesting that full oxidation is not achieved even at 5.0 sccm. In our previous work [11] an oxygen flow rate of 2.5 sccm was employed. It is now clear that this flow rate produces slightly oxygen deficient films, and that the results reported in that work are not necessarily indicative of fully oxidized $Mg_3(VO_4)_2$. Nevertheless, the extent of oxidation is clearly quite high at 2.5 sccm and the evidence presented for the formation of an (021) oriented film remains valid.

For fully oxidized films, only a single broad, featureless peak at 957 cm^{-1} is observed by FTIR (figure 4 (E) and (F)). As oxygen flow rate decreases this peak splits into two peaks at 967 and 924 cm^{-1} (figure 4 (D) and (C)). For an oxygen flow rate of 1.0 sccm, a third peak appears at 723 cm^{-1}. As the flow rate decreases to 0.3 sccm the 924 cm^{-1} peak shifts to lower frequency and increases in intensity relative to the 957 cm^{-1} peak, and the peak at 723 cm^{-1} shifts to 666 cm^{-1} and increases in intensity (figure 4(B)). In the absence of any oxygen, the two high frequency peaks are almost completely attenuated and the 666 cm^{-1} peak shifts to 715 cm^{-1} (figure 4(A)). The loss of intensity between 900 and 1000 cm^{-1} is of particular interest since this region corresponds to vibrational modes of VO_4 tetrahedra [2,17,18], which are present in $Mg_3(VO_4)_2$ but not in $Mg_3V_2O_6$ [2]. Thus, we conclude that the film deposited in the absence of oxygen contains little or no $Mg_3(VO_4)_2$, and is mainly composed of $Mg_2V_2O_6$. Similarly, the presence of VO_4 vibrational modes in the film deposited with 0.3 sccm O_2 suggests a mixture of $Mg_3(VO_4)_2$ and $Mg_3V_2O_6$. The correlation of the low frequency vibrational peak at 660–720 cm^{-1} with the presence of the $Mg_3V_2O_6$ (400) XRD peak (*cf.* figure 2)

suggests that the peak at 650–700 cm^{-1} arises from a vibrational mode of $Mg_3V_2O_6$. Similar results were obtained by Wang *et al.* [2].

Comparison of the FTIR spectrum of the fully oxidized film with that of $Mg_3(VO_4)_2$ powder reveals major differences, attributable to the high degree of orientation of the fully oxidized films. Evidently the orientation of certain bonds relative to the surface, coupled with the geometry of our FTIR reflectance accessory, prevents excitation of vibrational modes in the region between 600 and 800 cm^{-1} and alters the relative intensity of the modes above 800 cm^{-1}. A similar, though less dramatic effect was reported by Finke and Schrader for polymethylmethacrylate films [19].

The growth of the reduced $Mg_3V_2O_6$ phase from a fully oxidized ceramic target requires some explanation since conservation of mass dictates that the overall composition of the sputtered particles must equal the bulk composition of the target [20]. According to Waits [21], oxides are broken up into their component atoms and suboxides during sputtering. Oxygen often has a lower sticking coefficient on the substrate than the metal atoms and consequently the resultant films are oxygen deficient. Supplying additional oxygen in the gas phase during deposition reverses this effect and allows the deposition of fully oxidized films.

It is remarkable that the $Mg_3V_2O_6$ phase deposited in the absence of oxygen grows in a (100) orientation given the close relation between the $Mg_3V_2O_6$ and $Mg_3(VO_4)_2$ structures. Conversion from the orthovanadate to the reduced phase occurs through migration of the metal ions to different sites, but with retention of the cubic oxygen ion lattice (see figure 4 in [2]). As a result the structure changes from orthorhombic to cubic and the (021) planes in the orthovanadate phase become (111) planes in the reduced $Mg_3V_2O_6$ phase. This transformation was observed in our earlier work [11] where it was shown that severe reduction of a (021) oriented $Mg_3(VO_4)_2$ film results in formation of a (111) oriented $Mg_3V_2O_6$ film. Thus, one might expect that direct growth of $Mg_3V_2O_6$ on Au(111) would result in a (111) orientation rather than the observed (100) orientation. The observed formation of the (100) surface is most likely due to an unanticipated expitaxial relationship between the Au(111) and the $Mg_3V_2O_6$ (100) surfaces. In figure 5 we show an overlay of a cubic (111) surface with a cubic (100) surface having the same lattice parameter (the Au–Au bond distance in gold (2.86 Å) and the average O–O distance in $Mg_3V_2O_6$ (2.92 Å) are nearly identical). The match in the *x* direction is necessarily exact, but there is also an almost perfect coincidence between the two lattices in the *y* direction. After a distance of six lattice parameters in the *y* direction the vertices in the (111) and (100) surfaces line up with a mismatch of only 1.04%. The presence of this coincidence helps to explain the epitaxial formation of (100) rather than the (111) surfaces of $Mg_3V_2O_6$, although it is likely that other factors, including differences in surface free energy between the (100) and (111) surfaces, also play a role.

From the relationship between the structures of $Mg_3V_2O_6$ and $Mg_3(VO_4)_2$, one would expect oxidation of $Mg_3V_2O_6$ (100) to result in formation of an $Mg_3(VO_4)_2$ (001) surface. Attempts to oxidize the $Mg_3V_2O_6$(100) film in 50 Torr O_2 at 773 K for several hours failed to convert the $Mg_3V_2O_6$ (100) film into the orthovanadate. While XPS measurements show full oxidation of the $Mg_3V_2O_6$ (100) surface, XRD measurements continue to show the $Mg_3V_2O_6$ (400) peak with no evidence for the $Mg_3(VO_4)_2$ (004) peak. FTIR spectra show noticeable changes upon oxidation, including increased intensity in the region from 800 to 1000 cm^{-1} consistent with the formation of tetrahedrally coordinated vanadium. Thus, it is likely that some surface $Mg_3(VO_4)_2$ formation occurred during oxidation, but either the extent was not great enough to be observed in XRD, or the conversion did not occur with retention of the orientation of the cubic oxygen lattice.

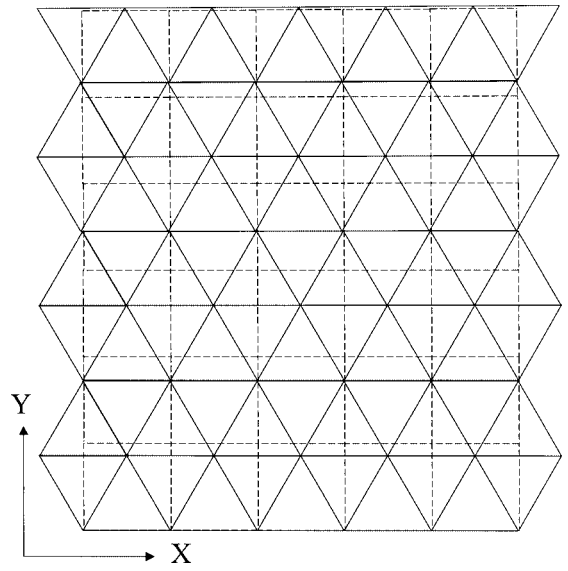

Figure 5. Schematic showing coincidence between (111) (solid lines) and (100) (dashed lines) fcc surfaces with identical lattice parameters.

4. Conclusions

By controlling oxygen flow rates during sputter deposition of $Mg_3(VO_4)_2$ on Au(111), films ranging from fully oxidized $Mg_3(VO_4)_2$ to highly reduced $Mg_3V_2O_6$ can be formed. Both phases exhibit an epitaxial relationship with the underlying substrate, with orthorhombic $Mg_3(VO_4)_2$ adopting an (021) orientation, while cubic $Mg_3V_2O_6$ adopts the (100) orientation. FTIR appears to be a sensitive probe of film oxidation. Continuous changes in the FTIR spectrum as the oxygen flow rate increases demonstrate that $Mg_3(VO_4)_2$ formation persists to very low oxygen flow rates, and that oxygen flow rates in excess of those used previously are required to achieve full oxidation. In a subsequent paper [13], we will detail the effects of exposure of these films to propane, oxygen, and propane/oxygen mixtures, demonstrate trends in behavior with increasing oxygen deficiency, and relate the results to the catalytic properties of these materials for propane ODH.

Acknowledgement

The authors thank Amitesh Maiti of Molecular Simulations, Inc. for providing the $Mg_3(VO_4)_2$ (021) image shown in figure 1, and Jim Miller of Sandia National Laboratories for providing the magnesium orthovanadate powder sample. This work is supported by the US Department of Energy under contract DE-AC04-94AL85000. Sandia is a multiprogram laboratory operated by Sandia Corporation, a Lockheed Martin Company, for the United States Department of Energy.

References

[1] J.G. Speight, *The Chemistry and Technology of Petroleum*, 2nd Ed. (Dekker, New York, 1991) p. 726.
[2] X. Wang, H. Zhang, W. Sinkler, K.R. Poeppelmeier and L.D. Marks, J. Alloys Compds. 270 (1998) 88.
[3] PDF card 19-0778, JCPDS – International Center for Diffraction Data, Newtown Square, PA.
[4] H.H. Kung, Adv. Catal. 40 (1994) 1.
[5] D. Siew Hew Sam, V. Soenen and J.C. Volta, J. Catal. 123 (1990) 417.
[6] X. Gao, P. Ruiz, X. Guo and B. Delmon, J. Catal. 148 (1994) 56.
[7] S.R.G. Carrazán, C. Peres, J.P. Bernard, M. Ruwet, P. Ruiz and B. Delmon, J. Catal. 158 (1996) 452.
[8] W. Weiss, M. Ritter, D. Zscherpel, M. Swoboda and R. Schlögl, J. Vac. Sci. Technol. A 16 (1998) 21.
[9] F. Libuda, F. Winkelmann, M. Bäumer, H.-J. Freund, Th. Bertrams, H. Neddermeyer and K. Muller, Surf. Sci. 318 (1994) 61.
[10] X. Xu, S. Oh and D.W. Goodman, Langmuir 12 (1996) 4877.
[11] J.A. Ruffner, A.G. Sault, M.M. Rodriquez and R.G. Tissot Jr., J. Vac. Sci. Technol. A 18 (2000) 1928.
[12] N. Krishnamachari and C. Calvo, Canad. J. Chem. 49 (1971) 1629.
[13] A.G. Sault, J.A. Ruffner, J.E. Mudd and J.E. Miller, in preparation.
[14] A. Burrows, C.J. Kiely, J. Perregaard, P.E. Højlund-Nielsen, G. Vorbeck, J.J. Calvino and C. López-Cartes, Catal. Lett. 57 (1999) 121.
[15] Ph. Courty, H. Ajot, Ch. Marcilly and B. Delmon, Powder Technol. 7 (1973) 21.
[16] A. Pantazidis, A. Burrows, C.J. Kiely and C. Miradatos, J. Catal. 177 (1998) 325.
[17] E.J. Baran, Monatsh. Chem. 106 (1975) 1.
[18] R. Iordanova, Y. Dimitriev, V. Dimitrov and D. Klissurski, J. Non-Cryst. Solids 167 (1994) 74.
[19] S.J. Finke and G.L. Schrader, Spectrochim. Acta 46A (1990) 91.
[20] K. Wittmaack, in: *Practical Surface Analysis*, 2nd Ed., Vol. 2, eds. D. Briggs and M.P. Seah (Wiley, New York, 1992) p. 124.
[21] R.K. Waits, *Thin Film Deposition and Patterning* (Am. Vac. Soc., New York, 1998) p. 92.